Supplementary Information for

Highly Robust Nanostructured Carbon Films by Thermal Reconfiguration of Ionomer Binding

Jae-Bum Pyo‡[a], Ji Hun Kim‡[a], and Taek-Soo Kim*[a]

[a] Department of Mechanical Engineering, KAIST, 291 Daehak-ro, Yuseong-gu, Daejeon 34141, Korea;

‡These authors contributed equally to this work.

*Corresponding author. E-Mail: tskim1@kaist.ac.kr

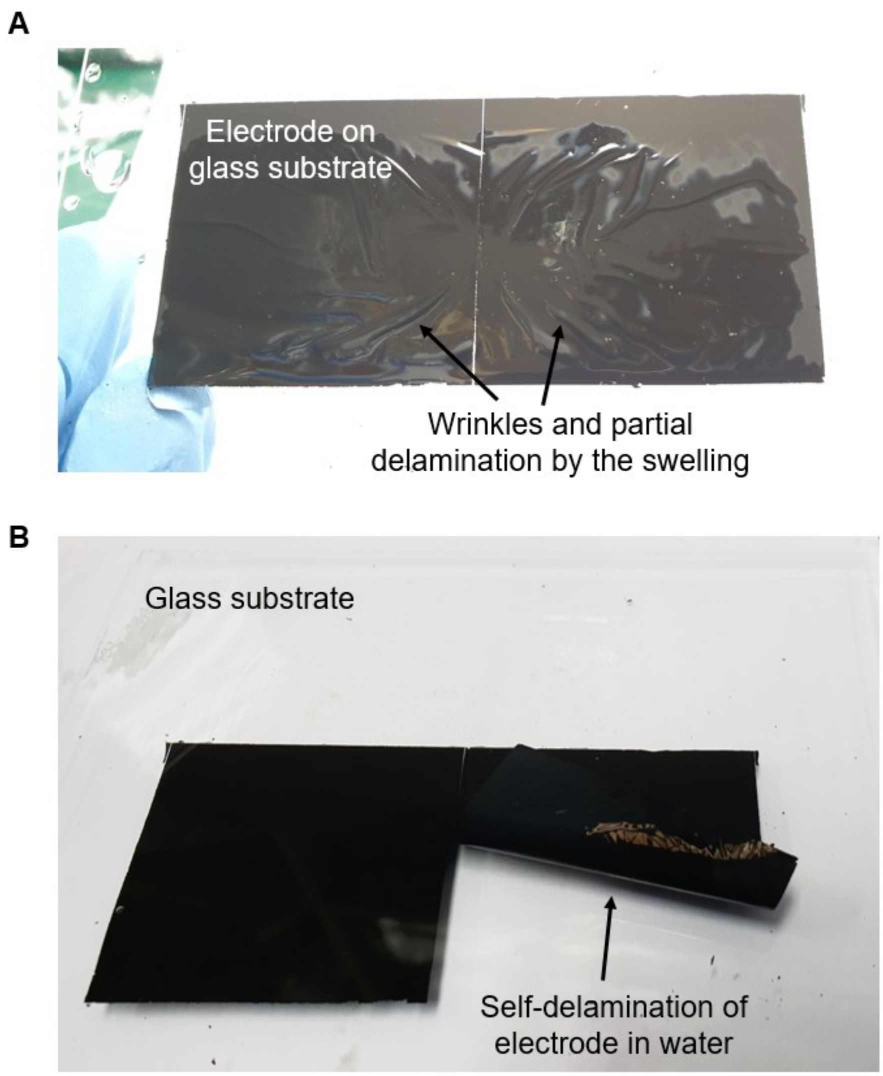

Fig. S1 Swelling-induced electrode separation. (**A**) Wrinkled and partially delaminated electrodes due to swelling mismatch. (**B**) The self-delaminated area became broader as the moisture absorption time increased.

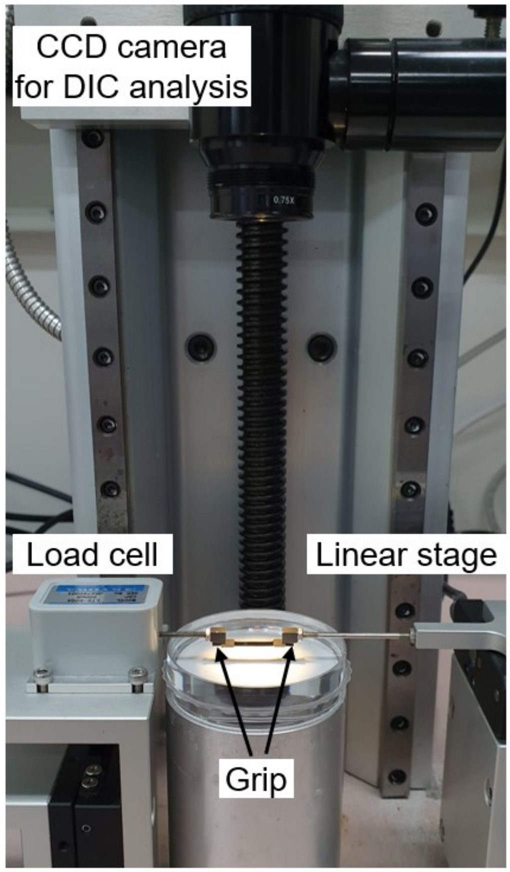

Fig. S2 Pseudo free-standing tensile testing system.

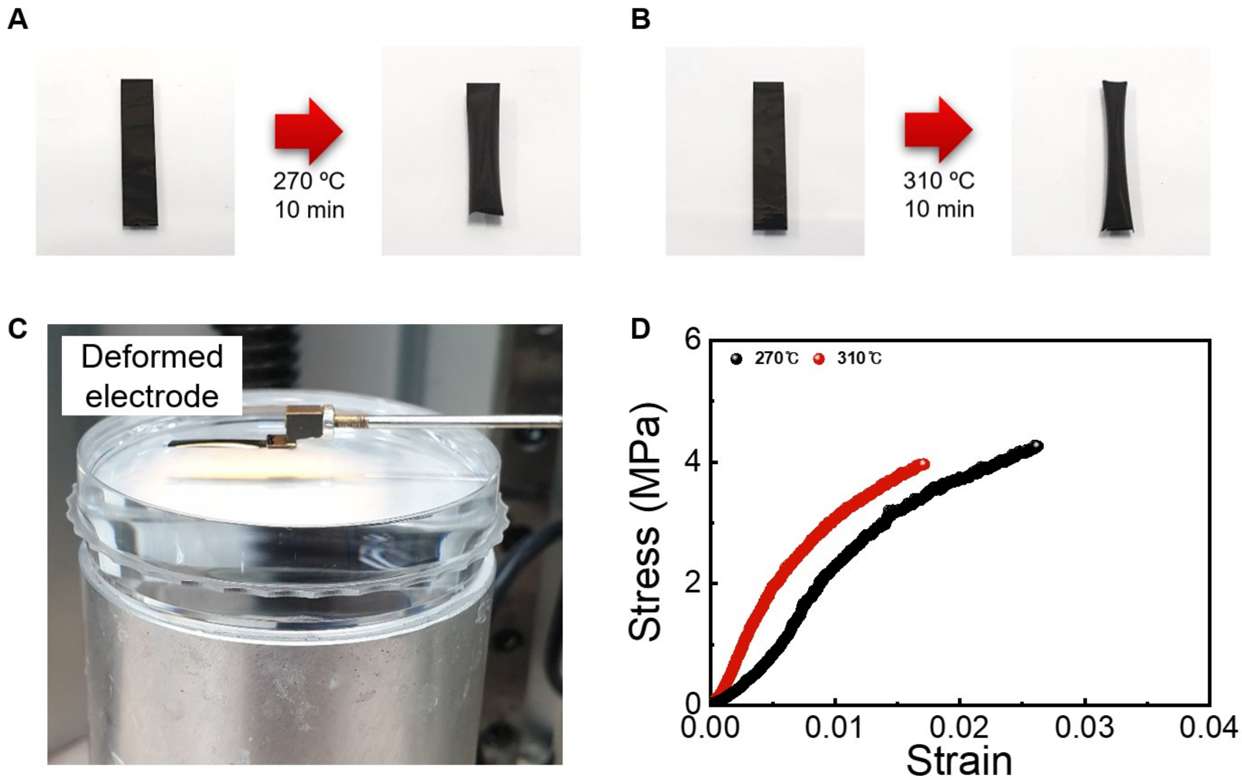

Fig. S3 Thermally reconfigured electrodes above 230 °C and tensile testing results. (**A**) Unstably deformed electrodes reconfigured at 270 °C and (**B**) 310 °C. (**C**) Deformed electrode attached on the gripping jig. (**D**) Stress-strain curves for the 270 °C electrode and the 310 °C electrode.

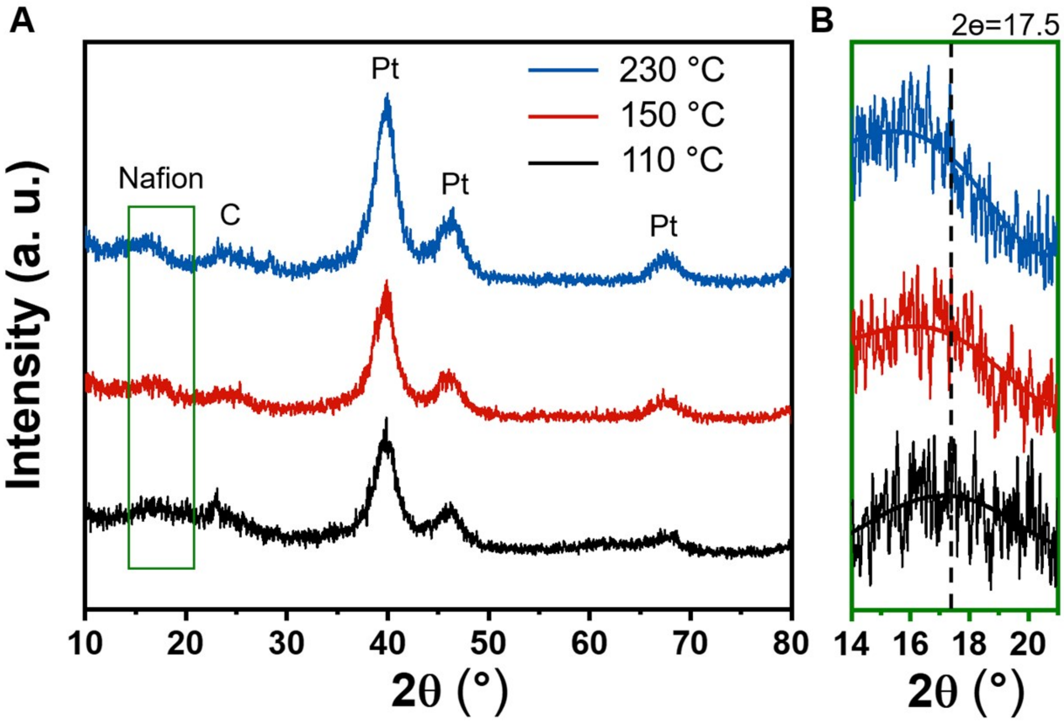

Fig. S4 XRD spectra as a function of the reconfiguration temperature. (**A**) XRD spectrum of each electrode treated at different temperatures. (**B**) Clarified the change of the crystalline morphology of the Nafion binder as the reconfiguration temperature increased.

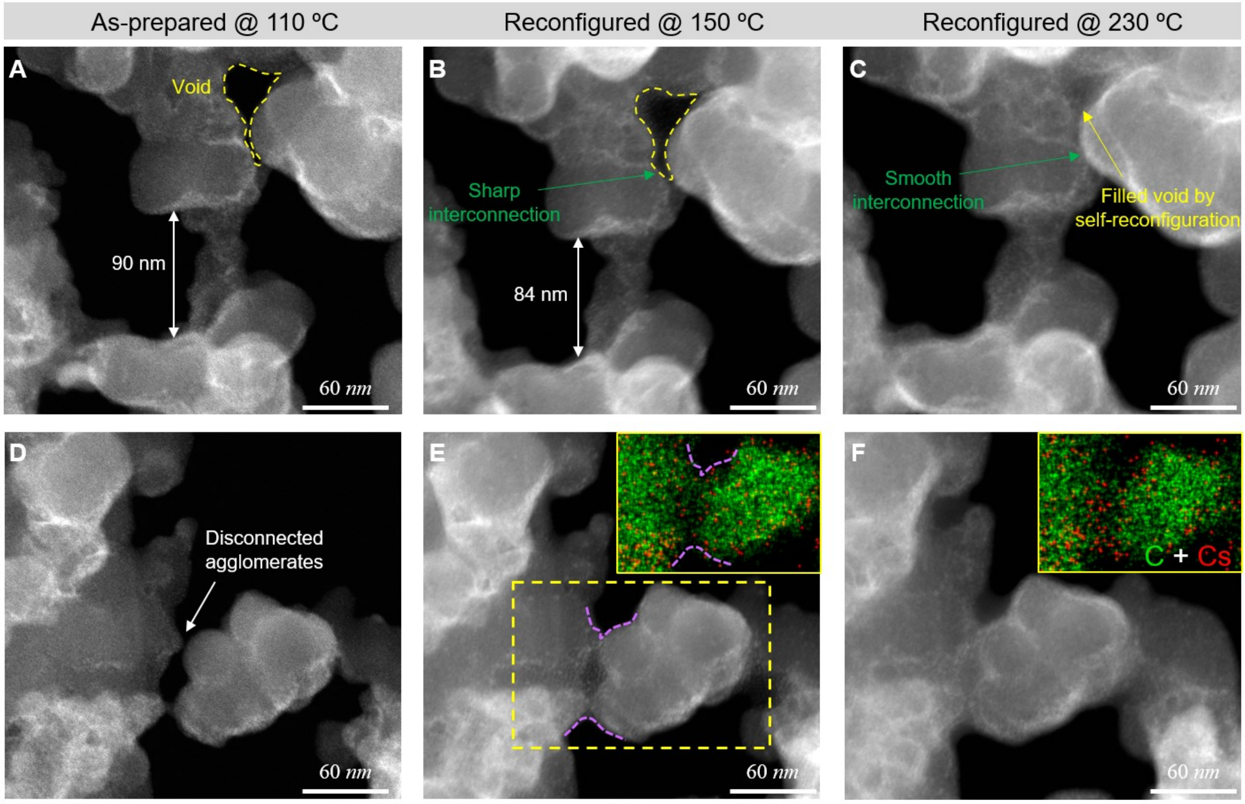

Fig. S5 HAADF-STEM images of the electrode with increasing reconfiguration temperature. (**A**) Nanostructure of the as-prepared electrode (110 °C). (**B**) Shortened distance between neighboring agglomerates reconfigured at 150 °C. (**C**) The reconfiguration at 230 °C promoted smooth interconnection and filled the small voids. (**D**) Neighboring agglomerates in the as-prepared electrode (110 °C) were initially disconnected. (**E** and **F**) The distance of disconnected agglomerates were shortened at 150 °C, but they still not sufficiently connected by Nafion binder (E). The inset shows elemental mapping of carbon (green) and cesium stained Nafion (red). Increasing the reconfiguration temperature to 230 °C allowed ionomer's melt flow in nanoscale (F).

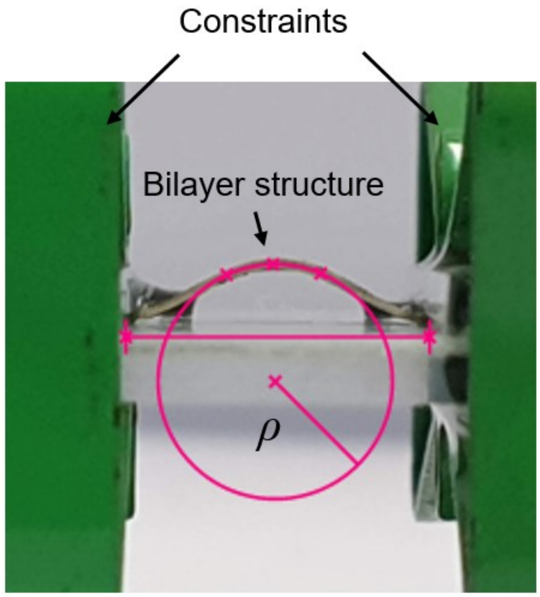

Fig. S6 Hygrothermal buckling of the bilayer structure.

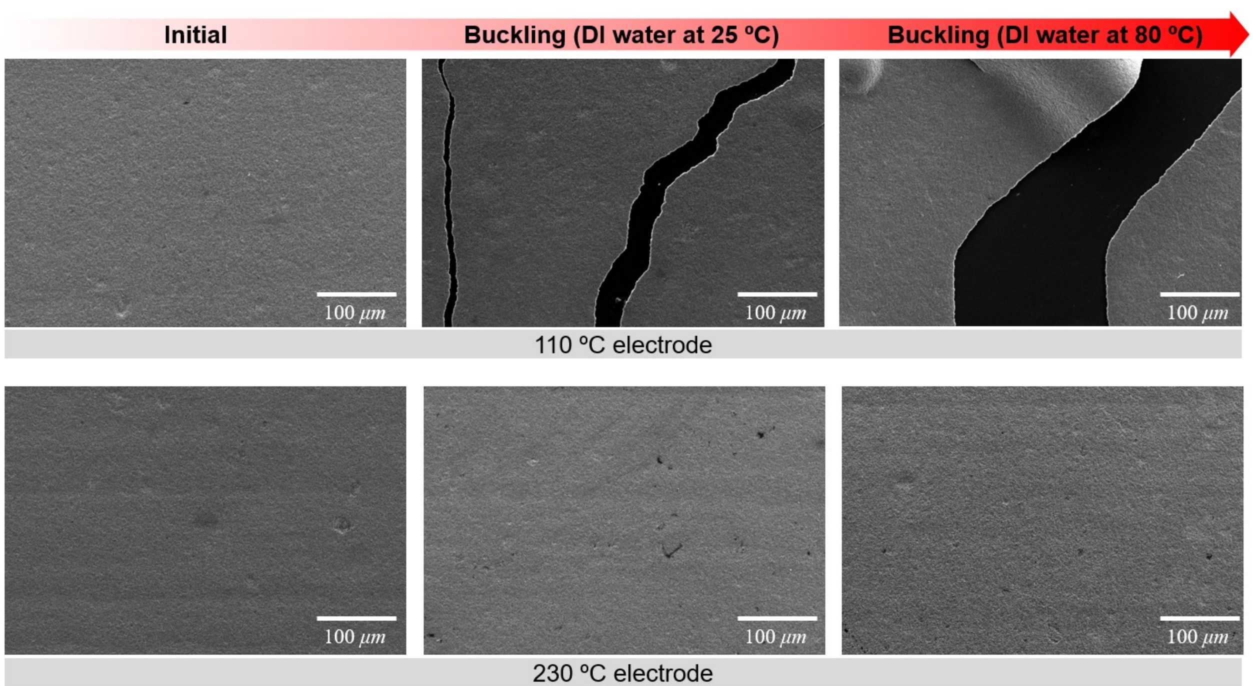

Fig. S7 Scanning electron microscopy images of 110 and 230 °C electrodes with increasing hygrothermal buckling loads.

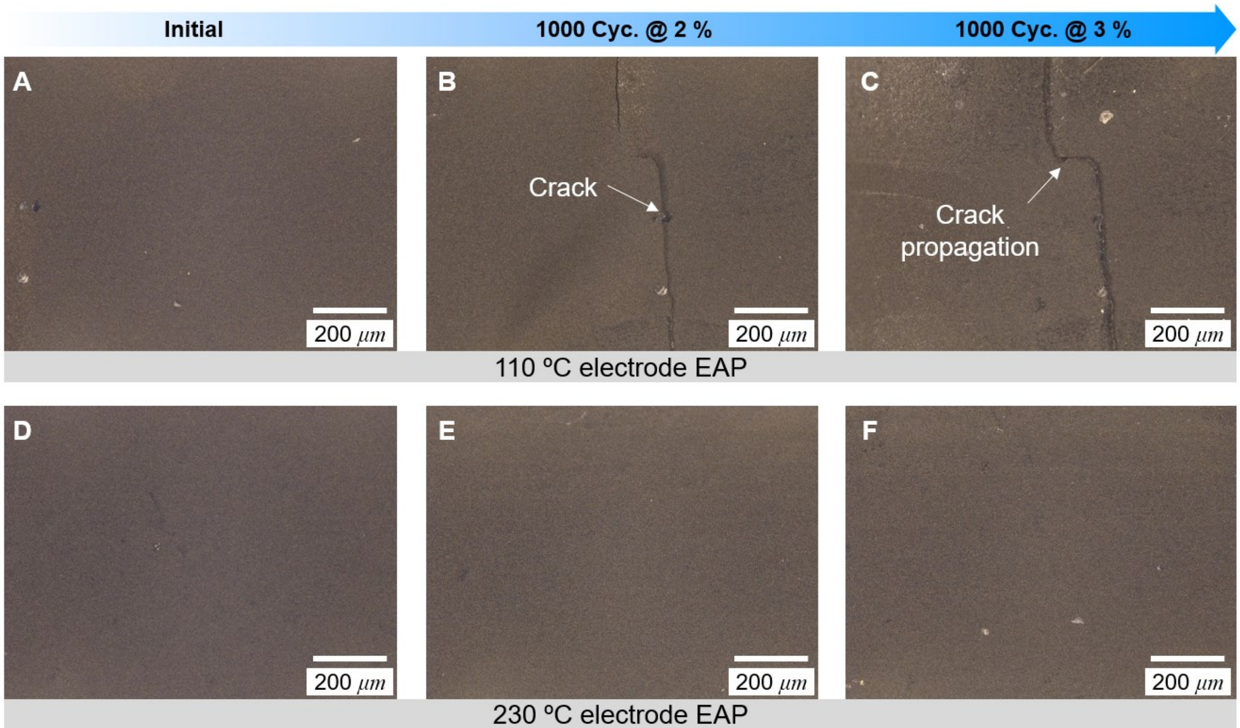

Fig. S8 Optical microscope images of 110 and 230 ºC electrode EAPs experiencing cyclic bending loads. (**A–C**) Initially, the 110 ºC electrode EAP was assembled without any defects (A). The cyclic loads at 2 % bending strain caused the electrode's crack (B), and this crack propagated as the strain increased to 3 % (C). (**D–F**) Initially, the 230 ºC electrode EAP was also assembled without any defects (D). This EAP demonstrated sufficient robustness to cyclic loads at 2 % (E) and 3 % (F) of bending strain, which is attributed to the higher mechanical strength.

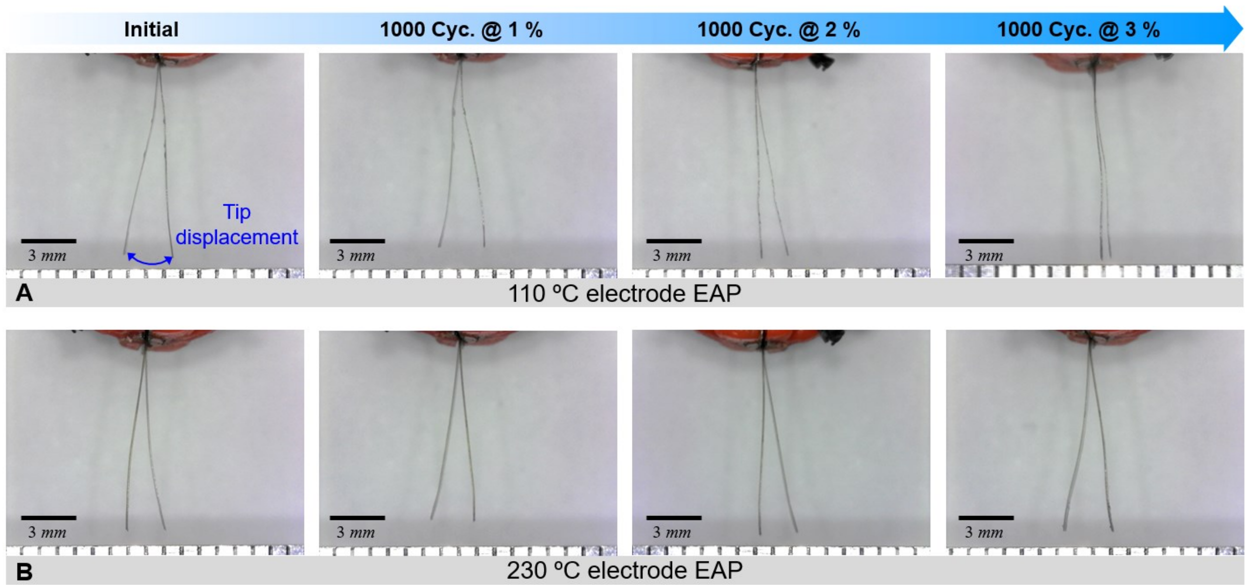

Fig. S9 Actuation performance affected by cyclic bending loads. (**A**) The 110 ºC electrode EAP showed degradation of the actuating displacement as the cyclic bending strain increased. (**B**) The 230 ºC electrode EAP maintained the initial actuating displacement, even after 3 % cyclic loads, which is attributed to sufficiently enhanced mechanical robustness.